JOURNAL OF AIRCRAFT
Vol. 46, No. 2, March–April 2009

Overview of the Cranked-Arrow Wing Aerodynamics Project International

Clifford J. Obara* and John E. Lamar†
NASA Langley Research Center, Hampton, Virginia 23681-2199

DOI: 10.2514/1.34957

This paper provides a brief history of the F-16XL-1 aircraft, its role in the High-Speed Research Program, and how it was morphed into the Cranked-Arrow Wing Aerodynamics Project. Various flight, wind-tunnel, and computational fluid dynamics data sets were generated as part of the project. These unique and open flight data sets for surface pressures, boundary-layer profiles, and skin-friction distributions, along with surface flow data, are described and sample data comparisons are given. This is followed by a description of how the project became internationally known as Cranked-Arrow Wing Aerodynamics Project International and is concluded by an introduction to the results of a four-year computational predictive study of data collected at flight conditions by participating researchers.

Nomenclature

C_p	=	pressure coefficient
c_f	=	local skin-friction coefficient
h	=	airplane altitude, ft
M_∞	=	freestream Mach number
R_n	=	Reynolds number based on aircraft reference chord of 24.7 ft
T	=	absolute temperature, °R
V/V_{RE}	=	ratio of velocity magnitude in boundary layer to that at the rake-extreme total-pressure tube
x/c	=	fractional distance along the local chord, positive aft
y	=	normal distance above the surface at a rake location, in.
y^+	=	Reynolds number like term for flat-plate turbulent boundary layer [1]
α	=	angle of attack, deg
β	=	angle of sideslip, deg
$2y/b_l$	=	fractional distance along the wing local semispan, positive toward the right-wing tip

Subscripts

avg	=	average value
nom	=	nominal value

Introduction

THIS paper provides a brief history of the F-16XL-1 aircraft, its role in the High-Speed Research (HSR) Program, and how it was morphed into the Cranked-Arrow Wing Aerodynamics Project (CAWAP). Various flight, wind-tunnel, and computational fluid dynamics (CFD) data sets were generated during the CAWAP [2]. These are described and sample data comparisons are given. This is followed by a description of how the project became internationalized and is concluded by an introduction to the results of a four-year CFD predictive study of data collected at flight conditions.

Presented as Paper 0487 at the 45th AIAA Aerospace Sciences Meeting and Exhibit, Reno, NV, 8–11 Jan. 2007; received 3 October 2007; accepted for publication 4 April 2008.

*CAWAP Project Engineer, Data Acquisition and Test Techniques Branch, Mail Stop 237. Member AIAA.

†CAWAP Principal Investigator, Configuration Aerodynamics Branch, Mail Stop 499. Associate Fellow AIAA.

CAWAP History

F-16XL Airplane

The F-16XL-1 airplane is a single-place fighter-type prototype aircraft developed by the General Dynamics Corporation's Fort Worth Division (now Lockheed Martin Aeronautics Company—Fort Worth) by stretching the fuselage of a full-scale development F-16A and adding a cranked-arrow wing, a modified fuel system, and a modified flight control system. There were 2 F-16XL aircraft built: F-16XL-1, which was used in the CAWAP, and a two-place version, F-16XL-2. Consequently, the terms F-16XL and F-16XL-1 are used interchangeably in this paper. Both aircraft had scheduled leading-edge flaps, elevons, and ailerons on the wing for control. The technical specifications for the airplane are given in Table 1, which is reconstructed from [2]. Details on the construction of the aircraft and its intended missions are given in [3–5].

The design of the cranked-arrow wing was a cooperative effort of the General Dynamics Corporation and the NASA Langley Research Center (LaRC). The new wing, common for both the F-16XL-1 and F-16XL-2 versions, was designed to provide the F-16 aircraft with improved supersonic performance while maintaining transonic performance that was comparable with that provided by the current F-16 design. As shown in Figs. 1 and 2, the resultant design had a leading-edge (LE) sweep angle of 70 deg inboard and 50 deg outboard of the crank. At the juncture of the wing leading edge with the fuselage, an S-blend curve was placed in the leading edge to alleviate a pitch instability that was found to occur at high angles of attack in wind-tunnel tests. All flight-test data reported in [2] were collected with the air dams (upper-surface fences mounted near the wing leading-edge crank) and wing-tip missiles installed, as shown in the figures.

HSR Program Overview

This program was started in 1990 to develop the technologies that would result in a supersonic passenger jet that would fly 300 passengers at more than twice the speed of sound while maintaining ticket prices that were comparable with current subsonic transports. As envisioned by the government and industrial partners, the high-speed civil transport (HSCT) would cross the Atlantic or Pacific Oceans in half the time of modern subsonic jets using new technologies for airframe manufacturing, propulsion systems, aerodynamics, and reduced environmental impacts. By 1995, based on several industry design concepts, computer modeling, and wind-tunnel tests, a Technology Concept Airplane was selected as a common reference point in furthering the technology development

Table 1 F-16XL-1 airplane specifications

Feature	Value
Wing span	32.4 ft
Height	17.606 ft
Length	54.155 ft
Reference chord	24.7 ft
Theoretical root chord	41.75 ft
Wing area	646.37 ft^2
Reference wing area	600 ft^2
Reference aspect ratio	1.75
Typical takeoff weight	35,000 lb
Engine max thrust	Pratt & Whitney F100-PW-200; 23,830 lb

process. This single concept was to have improved aerodynamic performance and operational characteristics while meeting environmental goals for emissions and noise pollution. The HSCT concept is depicted in Fig. 3.

Because of economic constraints, the program was phased out in fiscal year 1999. Despite the cancellation, the program still managed to meet or exceed many of the original HSR program goals. New high-temperature composite materials and structural concepts were developed to keep weight and manufacturing costs down while maintaining the strength and durability that would be required for the aircraft. NASA engineers developed new vision systems for the pilots that maintained safety and performance capabilities while eliminating the need for a drooped nose similar to the Concorde. Another critical element to the program was the development of a propulsion system that would not harm the environment in

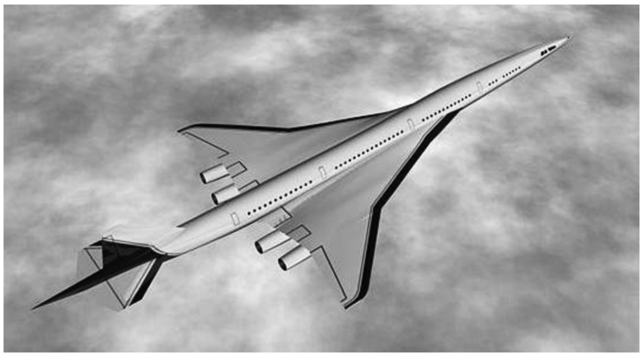

Fig. 3 High-speed civil transport concept.

atmospheric effects and that would mitigate the noise while providing the performance and durability required to keep the aircraft economically viable.

F-16XL Flight Overview and Planning for HSR

Early in the development of the HSR program, it was determined that improved aerodynamic performance while reducing the noise at high-lift conditions during takeoff and landing was a critical element to the program. The availability of the F-16XL aircraft with its cranked-wing configuration, which was similar to the HSCT concept, provided a unique opportunity for CFD correlation and code validation with flight and wind-tunnel data. The project was divided into three phases based on the required geometry changes to the basic aircraft. The phases are depicted schematically in Fig. 4 relative to the

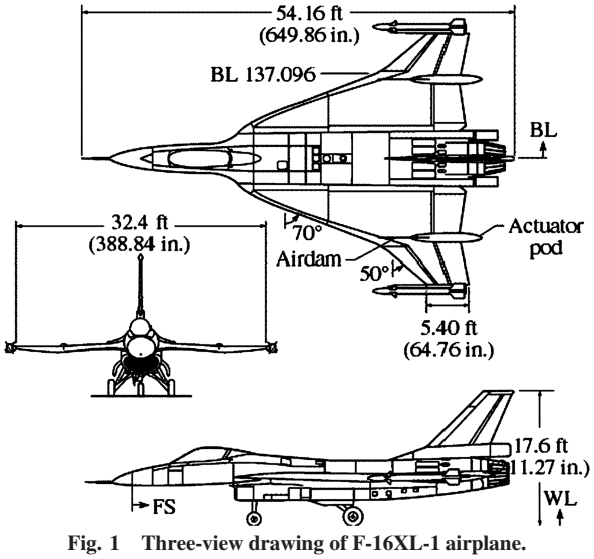

Fig. 1 Three-view drawing of F-16XL-1 airplane.

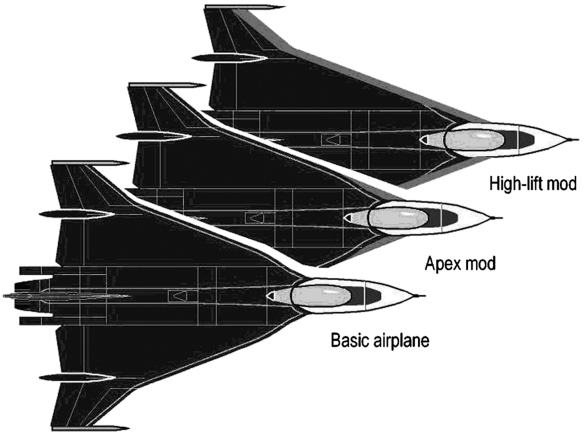

Fig. 4 F-16XL-1 research aircraft modifications.

Fig. 2 F-16XL-1 aircraft with missiles, tufts, modified flow-visualization paint scheme, and video targets (NASA photo EC96-43508-2).

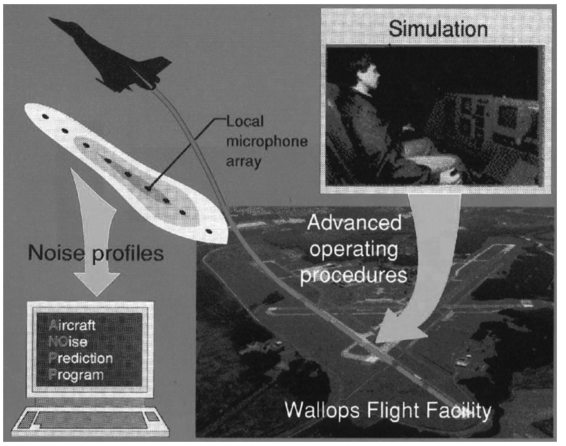

Fig. 5 Schematic of ground-to-flight correlation for assessing the impact of aerodynamic and operational concepts on noise profiles.

aircraft modification required. Phase 1 was the basic airplane with no modifications. This phase would serve as a baseline for the future modifications. Phase 2 required the removal of the S-curve in the apex region of the wing. This second configuration was more representative of the HSCT cranked wing. The third and final phase would incorporate a high-lift device along the entire leading edge of the aircraft. The exact configuration of the high-lift device would be determined from wind-tunnel experiments and CFD predictions. The high-lift configuration would be representative of the HSCT in a takeoff or landing configuration.

The primary objective of the flight-test project was to verify the performance of high-lift concepts while ensuring compliance with community noise standards. The first step was to establish a ground-to-flight correlation for the cranked-arrow wing planform. All three configurations would be flight-tested and the data would be used as a calibration of the design analysis tools as well as the noise-prediction codes. In addition, advanced operating procedures for takeoff and landing would be evaluated. The final objective was to assess integration and real-world operation of high-lift devices. A schematic of the ground-to-flight correlation is shown in Fig. 5.

CAWAP

During the phase 1 experiments on the baseline F-16XL aircraft in the spring of 1994, the remainder of the project as planned was cancelled due to funding limitations. Sufficient funding was provided to complete the first phase of the project, with a slight change to the objectives. This was the start of the CAWAP as it is known today. The revised objectives were to document upper-surface flow physics at high-lift and transonic test conditions and to

Table 2 Planned F-16XL CAWAP data comparisons

Item	Data comparison	Data type/instrument	Data source
1	On- and off-surface flow	Tufts	Flight
		Static pressures in a row	Flight
		Vapor screen	Flight
		Particle traces	CFD
2	Surface flow and pressure	Oil flow	Wind tunnel
		Pressure-sensitive paint	Wind tunnel
3	Surface pressure	Pressure-sensitive paint	Wind tunnel
		Calculations	CFD
4	Vortex-core location	Vapor screen	Wind tunnel
		Particle traces	CFD
5	Vortex-core location	Vapor screen	Flight, wind tunnel
		Particle traces	CFD
6	Surface flow	Oil flow	Flight
		Tufts	Flight
		Liquid crystals	Flight
7	Surface flow	Oil flow	Flight
		Tufts	Flight
		Particle traces	CFD
8	Surface flow	Oil flow	Flight, wind tunnel
		Particle traces	CFD
9	Surface pressure	Pressure-sensitive paint	Wind tunnel
		Particle traces	Wind tunnel
10	Off-surface flow	Vapor screen	Flight, wind tunnel
		Five-hole probe	Wind tunnel
11	On- and off-surface flow	Oil flow	Flight
		Vapor screen	Flight
		Particle traces	CFD
12	On- and off-surface flow	Oil flow	Flight, wind tunnel
		Vapor screen	Flight, wind tunnel
		Five-hole probe	Wind tunnel
13	Surface flow	Oil flow	Flight
		Tufts	Flight
		Liquid Crystals	Flight
		Propylene-glycol-methyl-ether traces	Flight
14	Surface flow	Oil flow	Flight
		Tufts	CFD
		Particle traces	Flight
		Propylene-glycol-methyl-ether traces	Flight
15	Vortex-core location	Vapor screen	Wind tunnel
		Dye traces	Water tunnel
		Particle traces	CFD
16	Surface pressure contours	Static pressures	Flight, wind tunnel
		Calculations	CFD
17	Surface pressure	Pressure-sensitive paint	Flight
		Static pressure in a row	Flight, wind tunnel
18	Surface pressure	Pressure-sensitive paint	Flight
		Static pressures in a row	Flight, CFD
		Static-pressure surface	CFD
19	On- and off-surface flow contours	Tufts	Flight
		Particle traces	CFD
		Stagnation pressure	CFD
20	Boundary-layer profile	Rake	Flight
		Velocities	CFD
21	**Skin-friction distribution**	**Modified Preston tube**	**Flight**
		Calculations	**CFD**
22	**Leading-edge boundary layer**	**Hot-film gauges**	**Flight**

Table 3 Actual F-16XL CAWAP data comparisons

Item [a]	Data comparison	Data type/instrument	Data source
3	Surface pressure contours	Pressure-sensitive-paint	Flight
		Calculations	CFD
6	Surface flow	Oil flow	Flight
		Tufts	Flight
		Liquid crystals	Flight
12a	On- and off-surface flow	Oil flow	Wind tunnel
		Vapor screen	Wind tunnel
16a	Surface pressure contours	Static pressures	Flight
		Calculations	CFD
17a	Surface pressure	Static pressure in a row	Flight, wind tunnel
18a	Surface pressure	Static pressures in a row	Flight, CFD
		Static-pressure surface	CFD
19	On- and off-surface flow	Tufts	Flight
		Particle traces	CFD
		Stagnation pressure contours	CFD
20	Boundary-layer profile	Rake	Flight
		Velocities	CFD
21	**Skin-friction distribution**	**Modified Preston tube**	**Flight**
		Calculations	**CFD**
22	**Leading-edge boundary layer**	**Hot-film gauges**	**Flight**

[a]Item numbers with "a" signify a reduction in the actual versus planned number of items being compared.

characterize the stability and control of the aircraft. The original intent of a flight, wind-tunnel, and CFD correlation experiment would be maintained, albeit for the baseline F-16XL configuration only. Table 2 illustrates the extensive set of planned comparisons between flight, wind tunnel, and CFD, and Table 3 provides the actual set of comparisons made. (These two tables are reconstructed from [2], with modifications from [2] shown in bold. The modifications are for additional comparisons that were overlooked at the time of the publication.)

Note that in Table 2 an attempt was made to perform off-surface laser-vapor-screen data using seeded material and to develop surface streaklines using propylene-glycol-methyl-ether. However, these two types of data were not obtained due to the lack of funding and higher-priority data sets that needed to be collected. Moreover, consideration was given to perform pressure-sensitive-paint studies in flight; however, it quickly became apparent that the timing and cost of the technological development was beyond the scope of this project. The concept was to use the laser light sheet in combination with a surface coating to obtain the pressure data, but it only reached the idea stage in a discussion between LaRC researchers and key personnel from the airframe industry. In addition, because the laser system was not funded to completion, this idea had to be abandoned.

Data Available from CAWAP

Seven different types of flight data were collected, as per Table 3, and four are shown schematically in Fig. 6. Three were pressure-based (surface static pressures, boundary-layer rakes, and modified Preston tubes [6]), three were video-recording-based (surface tufts, surface oil, and surface liquid crystals), and one was hot-film data. The pressure and surface flow data were used for the purpose of establishing the effects of variation in Mach number on the local flow. These data served as the basis for comparison with other data sets. The hot-film data were used to establish whether boundary-layer transition occurs and under what test conditions. Geometry data of the airplane upper surface were also obtained using photogrammetry and compared with the numerical surface description (see [2]).

Pressure Suite

Figures 6 and 7 detail the complete pressure-instrumentation system layout on the aircraft, including the distribution of the static ports by type, belt, or flush, and boundary-layer rakes or modified Preston tubes. These static ports are connected to internally mounted electronically scanning pressure (ESP) modules through tubes. Each pressure tube in the belt was used to measure two separate values of pressure. This was accomplished by sealing each tube about halfway along its length, thereby making provision for one forward and one aft port. The actual number of static ports associated with each belt is displayed in Fig. 7, imbedded along the belt nominal butt line (BL).

The flight surface pressures and corresponding flight-tuft images, along with boundary-layer rake and skin-friction data, are available in ASCII format in [7]. The pressures are ordered by flight number/test point and related to a particular flight condition through an accompanying table from [2].

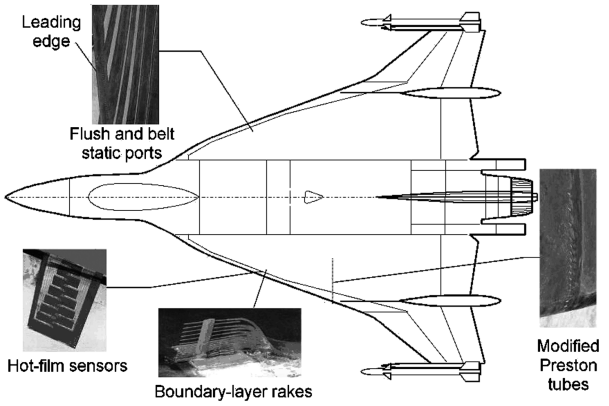

Fig. 6 Layout of pressure and hot-film instrumentation suite on the F-16XL-1 aircraft.

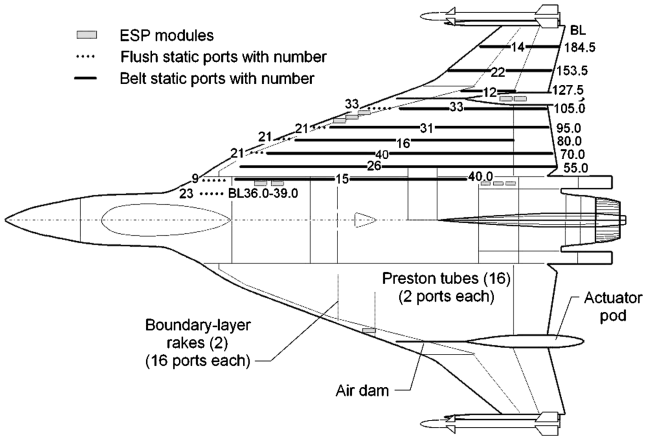

Fig. 7 Details of complete pressure-instrumentation suite and layout on the airplane.

The right-wing surface pressures (mostly upper surface) were measured using 337 static ports, both flush (LE region) and in streamwise belts, through 11 32-port ESP transducers (also called modules). Of these 337 ports, only 326 proved to be reliable and the distribution was 280 on the upper surface and 46 on the lower. The ports were arranged so that there would be a sufficient number at a given BL or fuselage station (FS) for cross plotting, as well as for covering other regions of special interest (i.e., the apex and ahead of/and behind the hinge lines of the trailing-edge control surfaces).

Boundary-layer measurements were made using two 2-in.-high rakes at a time at four different positions on the left wing, and the most inboard rake was always used as a control. Each rake used 16 active tubes (15 total pressures and 1 static pressure) of the 23 available. These two rakes were connected to one 32-port ESP module located inside that wing. When mounted on the aircraft, each rake was oriented into the local flow at an average angle over its height based on initial CFD predictions from the CFL3D code [8,9]. The flow conditions were for the complete aircraft (half-aircraft modeled with symmetry assumed) at $\alpha = 13$ deg, $M_\infty = 0.29$, and $R_n = 46.1 \times 10^6$ [i.e., flight condition (FC) 7]. (See Tables 4 and 5 for a listing of the FCs of interest in the current study and the associated flight and engine parameters, including those for FC 7.)

Figure 8 shows the four boundary-layer locations chosen: one well inboard of the shed-vortex systems (location 3), one underneath the primary vortex (location 4), and two associated with the secondary vortex. One of the latter is located underneath that vortex (location 5) and the other (location 7) is at its separation point; all are at a nominal position of FS 295. The average of the local flow at, and slightly off, the surface was used to establish the rake orientation angles for FC 7. This figure also shows the relative locations of the modified Preston tubes. They were to be located at the same fuselage station as the boundary-layer rakes, but a more aft position for the tubes was necessitated due to easier aircraft installation and to avoid the flow off a step in the leading-edge region.

The 16 modified Preston tubes (see Figs. 6 and 8) (the modification to each Preston tube is the integration of a static pressure port with the total-pressure tube) are used to determine local skin friction across the left wing near FS 330. These 32 pressures use the same ESP as the rakes, but not on the same flight. The tubes were aligned with the local flow using the same initial CFL3D solution at FC 7. The equation used to generate the experimental fluid dynamics (EFD) c_f values comes from [5] and relates, through a process of calibration, the pressure change between the total and static tubes to the local skin friction.

Video Suite

Video data were recorded with up to six external cameras: two mounted atop the vertical tail, one on either side of the fuselage behind the canopy, and one in the nose of each dummy missile. An internally mounted head-up-display camera was also used on occasion. Figure 9 shows the camera locations on the aircraft. The time was added to each image by a time-code inserter so that the images could be compared to form a composite and so that the flight-test conditions could be established. Images of interest were digitized in a 512 by 480 pixel format for further processing so that quantifiable video data could be developed. In addition to the images, the other input quantities needed for the processes were the video targets and the position and calibration characteristics of each camera/lens combination.

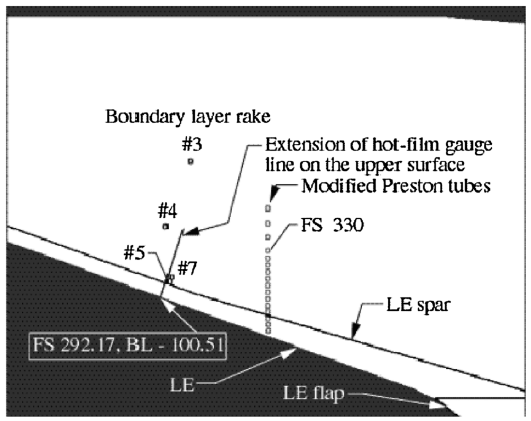

Fig. 8 General arrangement of rake and modified Preston tube relative locations on F-16XL-1 left wing; pressure instruments oriented for $M_\infty = 0.291$, $\alpha = 13$ deg, and $R_n = 46.1 \times 10^6$.

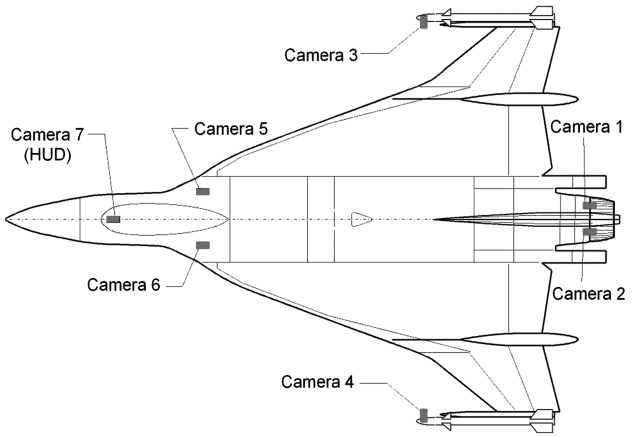

Fig. 9 Locations of the video suite on the F-16XL-1 airplane (HUD denotes the head-up display).

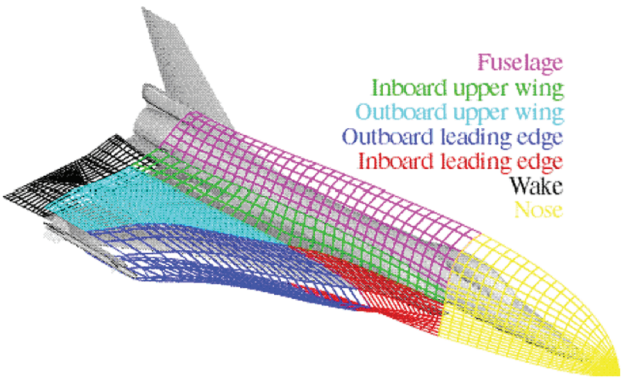

a) Inner

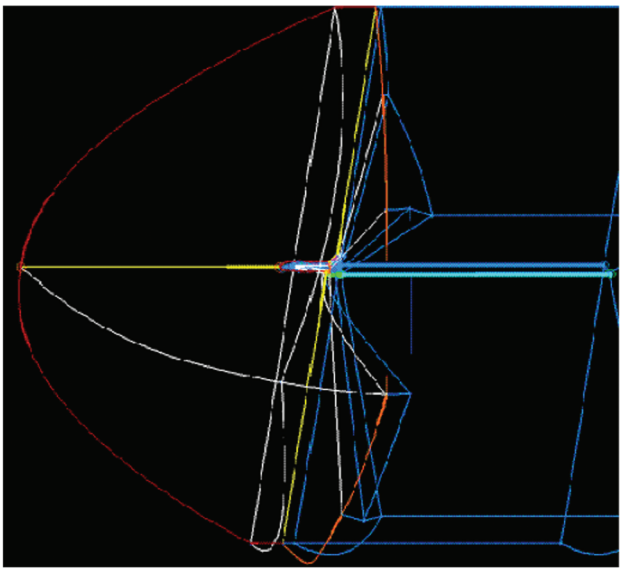

b) Outer

Fig. 10 CFD block structure layout for F-16XL-1.

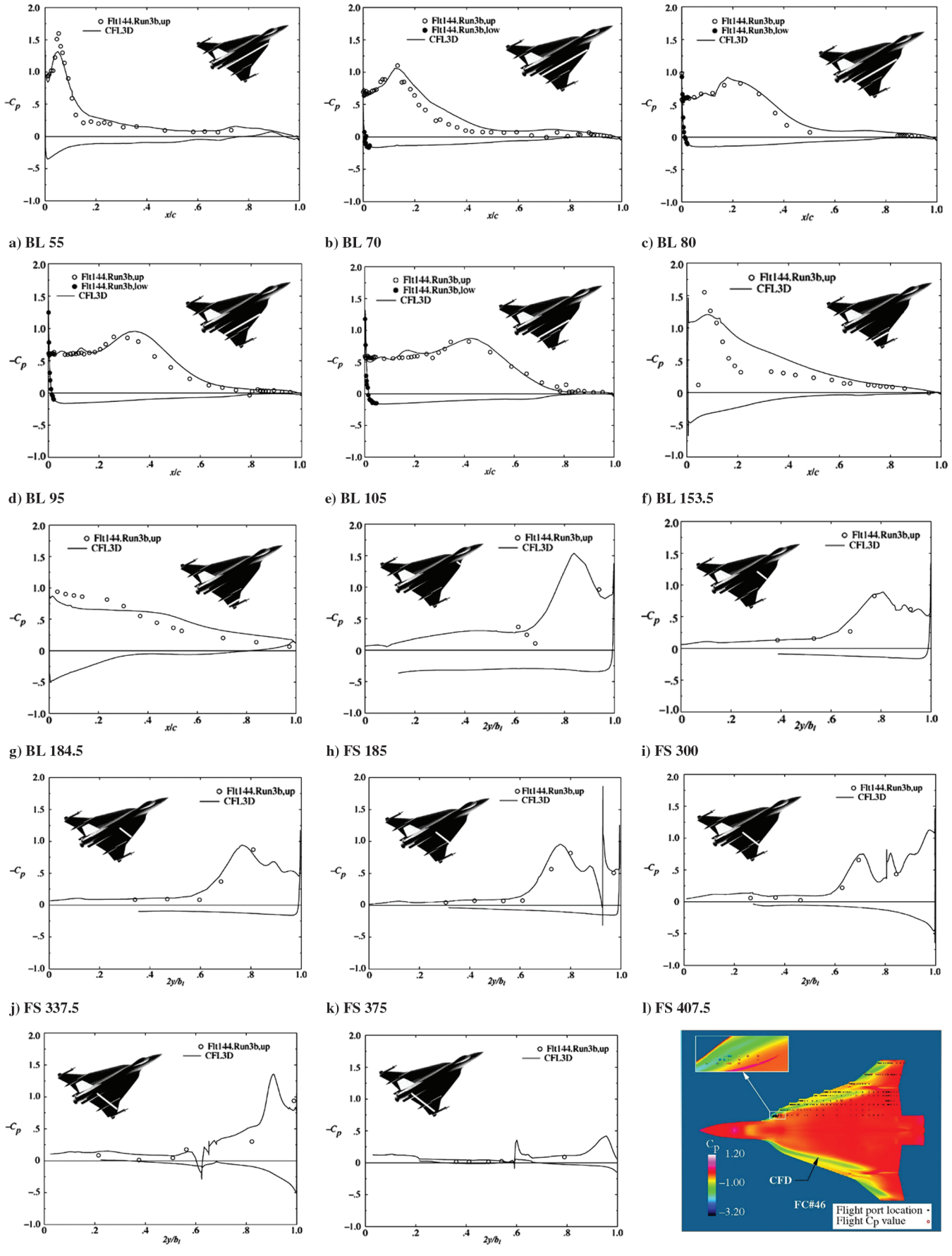

a) BL 55 b) BL 70 c) BL 80

d) BL 95 e) BL 105 f) BL 153.5

g) BL 184.5 h) FS 185 i) FS 300

j) FS 337.5 k) FS 375 l) FS 407.5

m) FS 450 n) FS 492.5 o) Upper surface Cp distribution

Fig. 11 CFD (CFL3D) and measured C_p at FC46 ($M_\infty = 0.527$, $\alpha = 10.4$ deg, and $R_n = 46.9 \times 10^6$) from [2].

Wind Tunnel

The second major source of data was from wind-tunnel tests with a variety of model scales. Some of these wind-tunnel tests were conducted on the F-16XL configuration before the HSR program and others were done in direct support. These tests encompassed a variety of configurations at various Mach and Reynolds numbers. Because some of the tests were conducted with the air dams not installed, they were not applicable for comparison with flight data. The following three wind-tunnel tests were primarily used for the flight and CFD comparisons.

1) A test on a 0.11-scaled model was conducted in the NASA Ames Research Center's 11 ft tunnel before the start of the flight project. The test is described in [10], and the actual data are tabulated in [11]. This model was specifically built to estimate the airloads for the airplane from $M = 0.60$ to 2.0 using 190 pressure ports distributed on the left-wing upper surface and the right-wing lower surface. The Reynolds numbers tested were 2.3×10^6 and 2.75×10^6, and the angle of attack varied from -1.94 to 28.75 deg. The ports were located in streamwise rows that did not nominally match the airplane. Because of data release restrictions, no direct comparisons were made with flight or CFD results. However, unscaled transonic pressure coefficient contours were used for comparison purposes in [2].

2) The test for the 0.18-scaled model was conducted in the LaRC 30 by 60 ft tunnel at a Mach number of less than 0.08 and a Reynolds number of 2.1×10^6. The angle of attack varied from -5 to 30 deg and the angle of sideslip varied from -20 to $+20$ deg. In addition to force/moment and pressure data, some vapor screen images were captured. A set of pressure results was published [2] and the force/moment results were published in an earlier paper [12]. The basic model has 30 right-wing flush upper-surface ports located to yield pressures for both streamwise and spanwise rows. The ports are nominally duplicated on the airplane for comparison. Only two runs were used from this test for comparison: one was a force/moment and the other was a pressure, both at 0 deg sideslip.

3) The third wind-tunnel test used for comparison was a 0.04-scaled model in the LaRC Basic Aerodynamic Research Tunnel (BART). The test conditions included Mach numbers less than or equal to 0.165, Reynolds numbers less than 1.12×10^6, and an angle-of-attack variation from 5 to 20 deg. This model had 82 pressure ports divided between the right upper-wing surface and the left lower-wing surface. The pressure ports correlated with the 0.18-scaled model as well as being nominally duplicated on the airplane. Selected results from the BART test appear in [13], in which they have been compared with Euler code predictions.

CFD Modeling

The last major source of data was that generated by CFD [2]. The flow solver CFL3D was run in the Navier–Stokes mode with a turbulent boundary-layer employing the Baldwin–Lomax with the Degani–Schiff turbulence model (in the j–k directions) on a multiblock patched grid over a variety of wind-tunnel and flight-test conditions (see [8,9]). Two separate grids were used to model half of the aircraft configuration (with undeflected control surfaces) and external flowfield. The initial grid had 36 blocks and was used with version 3 of the flow solver to produce the initial results upon which the locations and orientations of the surface instrumentation were set. The current grid had only 30 blocks and was used with version 5 of the flow solver to obtain the comparative solutions reported herein.

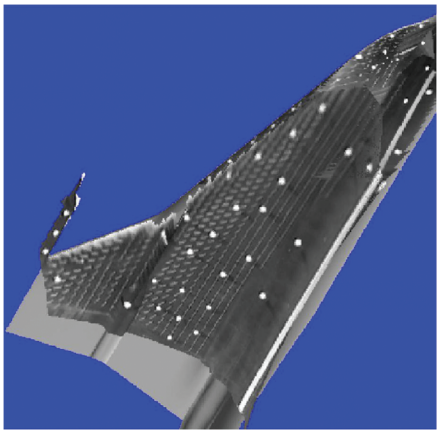

a) Tuft images projected from three cameras onto aircraft grid

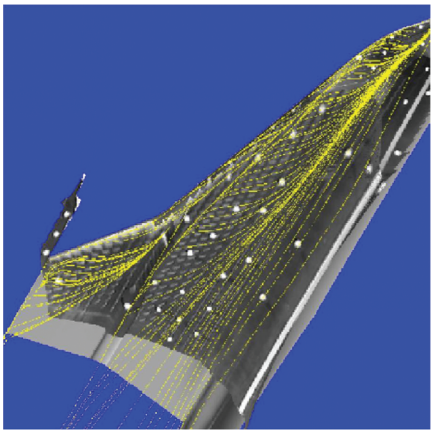

b) Combination of tuft images and CFD surface streamlines

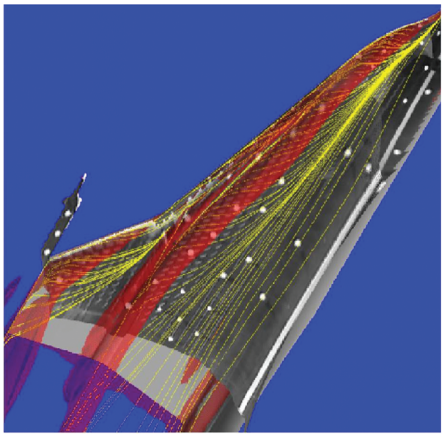

c) Combination of tuft images, streamlines, and vortex systems

Fig. 12 Flight tuft data from three cameras on F-16XL-1 airplane and CFD solution at FC46 ($M_\infty = 0.527$, $\alpha = 10.4$ deg, and $R_n = 46.9 \times 10^6$) from [2].

The current grid was needed for two reasons: namely, to have the grid more closely conform to the actual fuselage and wing geometries and to improve the grid layout on the wing and fuselage surfaces. The missile- and missile-rail grids were effectively the same with either grid. For the current grid, the inner region of the aircraft was modeled by 16 blocks, the outer region was modeled by 14 blocks, and all 30 blocks are shown schematically in Fig. 10. The boundary conditions were symmetry, a solid wall for the outer mold lines, flow into the duct inlet (but the exhaust face was faired over), and Riemann-type conditions at the far-field boundaries. A total of 1,372,096 cells (1,707,117 node points) were used to obtain solutions at specified test conditions (M_α, α, grid R_n, T, etc.). To maximize computer-resource allotments, the minimum number of cells was used. The resulting grid spacing normal to the numerical surface led to a value of y^+ of 2 at wind tunnel R_n, whereas at flight R_n the average value was y^+ of 82. In an effort to compensate for the insufficient grid spacing at flight conditions, the wall function option was used to augment the turbulence model in CFL3D. The wall function is defined as that boundary-layer growth rate expected from a turbulent mean flow near the wall [14].

Database of Results

A database was set up, as described in Appendix B of [2], to facilitate data comparison between the various CAWAP sources (i.e., flight, wind-tunnel, and CFD). The data types used for comparison were local surface pressures between the three sources and boundary layer and skin friction between the flight data and CFD predictions. Moreover, the database stored administrative information about the tests (metadata) and the full (mass storage) path name of the resulting data files. For the EFD measurements, the data stored are files of pressure, force/moment, still photographs, and two-dimensional images digitized from videotape (both instantaneous and time-averaged); for CFD predictions, the grid and solution files are stored as well as C_p data at selected FSs and BLs. The F-16XL-1 database also supports the viewing of 3-D renderings of the 2-D flight images through computer software tools. Queries for selected pressure data and 2-D flight image data were available to internet users by completing an appropriate online form on this unclassified/unlimited server. The Web service was functional at the publication time of [2] and shortly thereafter, but has since been discontinued due to changes in policies and available resources.

Sample CAWAP Comparisons

Selected figure samples from the CAWAP report [2] are repeated as Figs. 11–14. Following each set of figures is an associated commentary provided for completeness. Note that these figures may contain a legend signifying which flight and test point (run number) served as a source for the flight data: for example, Flt144.Run3b, up.

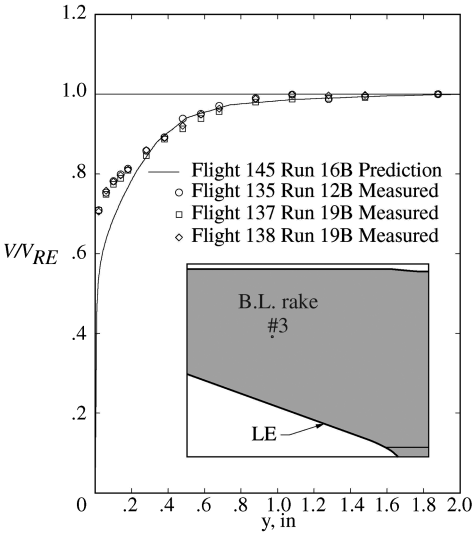

a) Rake 3: FS 302.17, BL –52.93

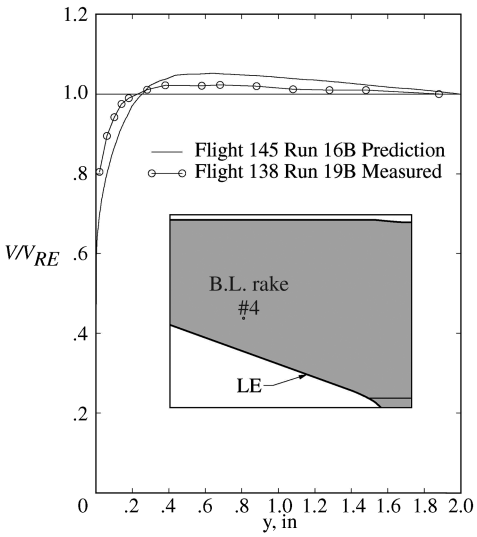

b) Rake 4: FS 293.45, BL –76.22

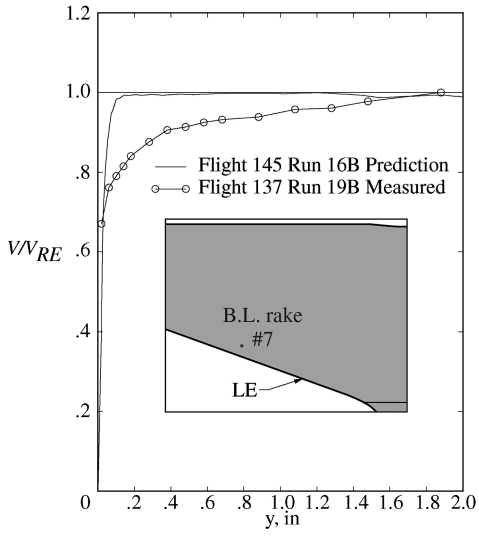

c) Rake 7: FS 295.52, BL –94.33

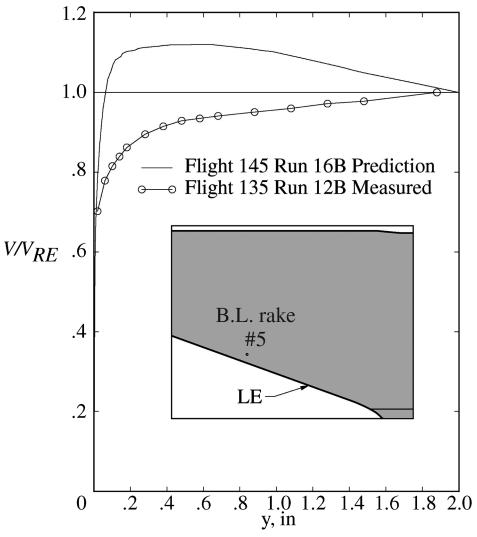

d) Rake 5: FS 294.59, BL –96.06

Fig. 13 Predicted and measured velocity profiles for boundary-layer rakes on F-16XL-1 airplane for FC 7 ($M_\infty = 0.29$, $\alpha = 11.89$ deg, $\beta_{\text{nom}} = 0$ deg, $h = 5000$ ft, and $R_n = 44.4 \times 10^6$) from [2].

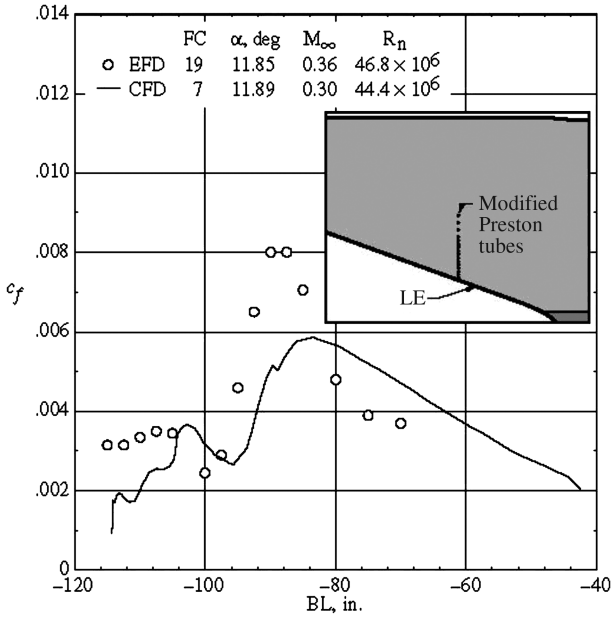

Fig. 14 Predicted and measured c_f on F-16XL-1 airplane at FS 330 for FC19/FC 7 ($M_{avg} = 0.33$, $\alpha_{avg} = 11.9\,deg$, $\beta_{nom} = 0\,deg$, and $R_{n,avg} = 45.6 \times 10^6$) from [2].

These data-set associations are not the same as the FC, but each one shown has a FC equivalent, as per the figure caption.

Figures 11a–11n show good overall agreement between the measured and predicted results at this flight condition. There are, however, three notable exceptions. The first exception is that the primary vortex effect on the suction peak at BL 55, the most inboard location, is underpredicted. The second exception is at BL 153.5, in which the measured data have the primary-vortex suction peak more forward than predicted and are followed by a more rapid compression downstream. The final exception is the unusual and uncharacteristic variation near $2y/b_l = 0.6$ for FS 185. The associated ports for the latter are located in and toward the aft-end portion of the S-blend curve part of the airplane, a region in which the flow is very sensitive. Even with this unusual behavior of C_p, these results are retained because they do bracket the predicted data at this FC.

Figure 11o provides an overview of the upper-surface C_p comparison in which the black dots represent the location of the flight ports and the associated color of the surrounding bubble indicates the measured value. When the color of the bubble is the same as the background CFD solution, only the black dot is noted. Generally, good overall agreement is seen, except in the S-blend region, in which the measured pressures are more negative, but elsewhere the differences are such that the measured values are more positive.

Figure 12 shows the fusion (overlaying) of surface-tuft images from the three left-side cameras (tail, missile nose, and fuselage apex) with CFD surface streamlines and vortex-core representation for FC 46. (The white circles are video targets used for camera registration.) In particular, Fig. 12a presents the camera combination obtained by using the video targets with camera location and orientation angles. Figure 12b shows that the CFD surface streamlines compare well with the flow depicted by the surface tufts. Figure 12c shows the addition of the stagnation-pressure isosurfaces (at a value of 0.78, representing the locations and extent of the various airplane vortex systems) with transparency. As expected from the results of the surface comparison, the vortex system is well located with respect to the flight tufts [2].

Figure 13 shows the boundary-layer (B.L.) profiles of measured and predicted data. The profile for B.L. rake 3 is seen in Fig. 13a to be that of a classical streamwise flow, and this location was measured on all such flights to be used as a control. This figure shows good data repeatability and that the predictions agree well with them away from the wall. The data presented in Fig. 13b for B.L. rake 4, underneath the primary vortex, show that the predicted trends are seen in the measured data, including the y location for the onset of jetlike flow followed by a reduction from there to the rake extreme. Figures 13c and 13d are associated with the secondary vortex, one underneath the core (rake 5) and one along the secondary separation line (rake 7). Two points are highlighted with respect to these two rake data sets: the predicted values do not match the measured ones, but do show how the anticipated flows would impact the boundary-layer profiles, and for all practical purposes, the two measured data sets are the same with a profile that does not asymptote to the boundary-layer rake-extreme value.

Figure 14 shows the predicted and measured local skin-friction coefficient at FS 330 for FC 7 and FC 19, respectively, as these FCs were quite close. High skin-friction peaks are an indication that a vortex system is present above the surface. Both sets of data show at least two such peaks. The predicted values for the primary (inboard) vortex have a different trend and reach a lower value than the measured data, and the vortex location is predicted more inboard than that measured: ∼BL-90; however, the solution does a somewhat better job at estimating the peak value and location of the secondary vortex, albeit with two unexplained oscillations that trail toward the LE (∼BL-116).

CAWAP International

Organization

At the 2000 Research and Technology Organization/Applied Vehicle Technology (RTO/AVT) Symposium held in Braunschweig, Germany, this international group was asked whether there was interest in predicting the flight results around the F-16XL aircraft, as the report [2] documenting the work was in the process of being readied for publication. As a consequence, the

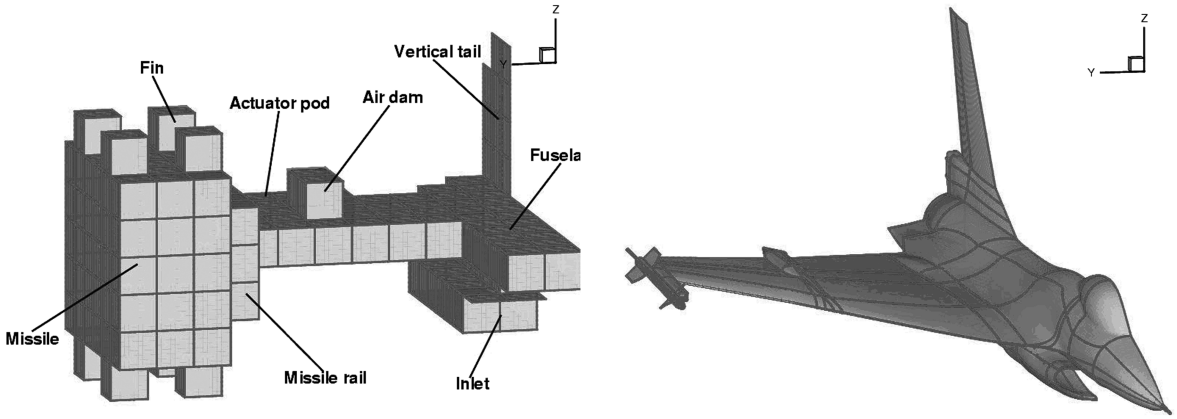

Fig. 15 Abstraction of the surface geometry (left) and projected abstraction (right) for the F-16XL half-span model from Boelens et al. [19]. [Structured (pictured) and unstructured grid development from the IGES file is discussed in this paper].

Performance, Stability & Control and Fluid Physics Technical Committee established an exploratory team to assess interest among the member nations on this and related topics. During the ensuing year, a team was constituted and at their first meeting in Loen, Norway, in the spring of 2001 they examined a variety of vortical-flow topics that could lead to task groups or symposia. A total of five topics were offered for consideration. Some went forward individually, whereas others were combined to gain AVT Panel recommendation for acceptance and Research and Technology Board (RTB) approval.

In particular, two topics presented at the Loen Symposium on Vortex Flows and High Angle of Attack, during the 2001 spring RTO meeting week, were put forward separately for further study. They were the CAWAP [15] and the Vortex Flow Experiment number 2 (VFE-2) [16], both of which dealt with vortical flows around slender wings. In the fall of 2002, these two topics were merged into a single proposal that the AVT Panel could recommend for approval by the RTB. Success was achieved in the spring of 2003 when the RTB granted approval for AVT-113 and authorized its first meeting to commence during the upcoming RTO/AVT Symposium week. The title of the task group was "Understanding and Modeling Vortical Flows to Improve the Technology Readiness Level for Military Aircraft." Even though integrated, each topic had its own facet lead, and these leaders became the cochairmen of the task group. The title for the expansion of CAWAP activity to the International aerodynamics community within the RTO was denoted as CAWAP International (CAWAPI). This name was crafted in advance in anticipation of approval and involved using a virtual laboratory (VL) at LaRC for facilitating secure data storage and transmission (see [17,18]).

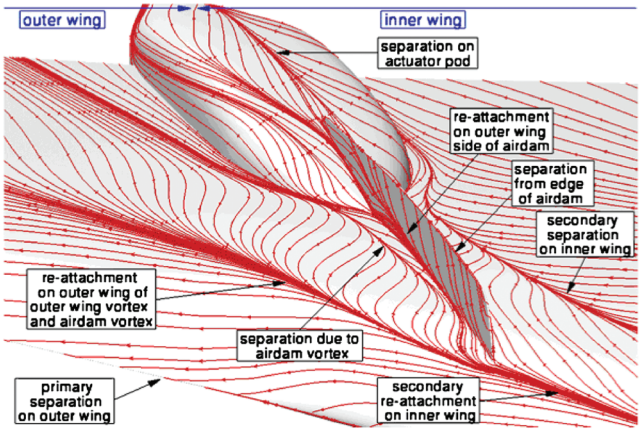

Fig. 16 Surface streamlines with interpretation for FC 7 with ENSOLV solver from Boelens et al. [20].

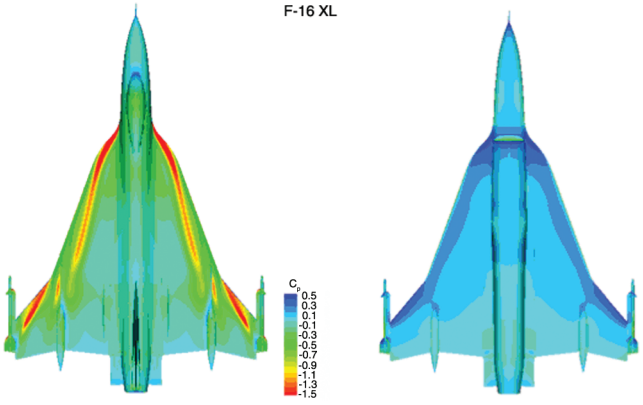

Fig. 17 Upper- and lower-surface C_p results for FC 7 with PMB solver from Badcock [21].

Features

The features of the CAWAPI are contained in the foundational document for the task group known as the "Terms of Reference": an internal RTO/AVT Panel document. In particular, there are basically

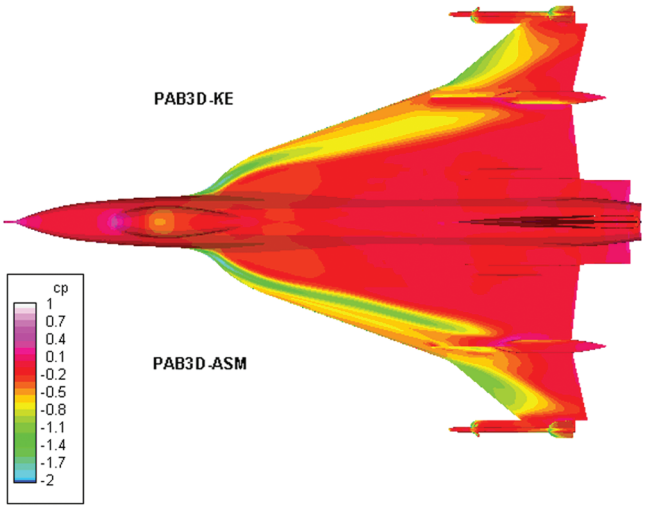

Fig. 18 Turbulence modeling effect on C_p for FC46 with PAB3D solver from Elmiligui et al. [22].

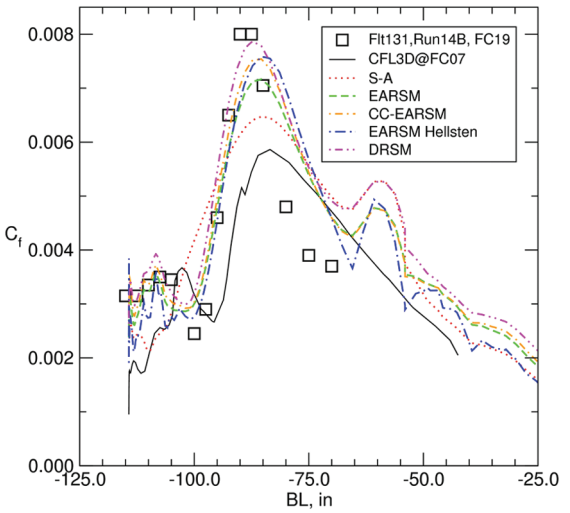

Fig. 19 Turbulence modeling effect on C_p for FC19 with Edge solver from Goertz and Jirásek [25].

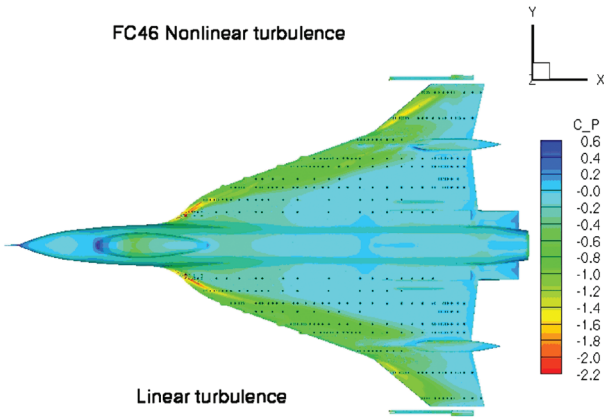

Fig. 20 Turbulence modeling effect on C_p for FC46 with USM3D solver from Lamar and Abdol-Hamid [29]. (Flight data represented by small circles surrounding the pressure-port locations, shown as black dots, are colored by the CFD C_p scale. Agreement between the two sets is good when no discernible color difference is noted.)

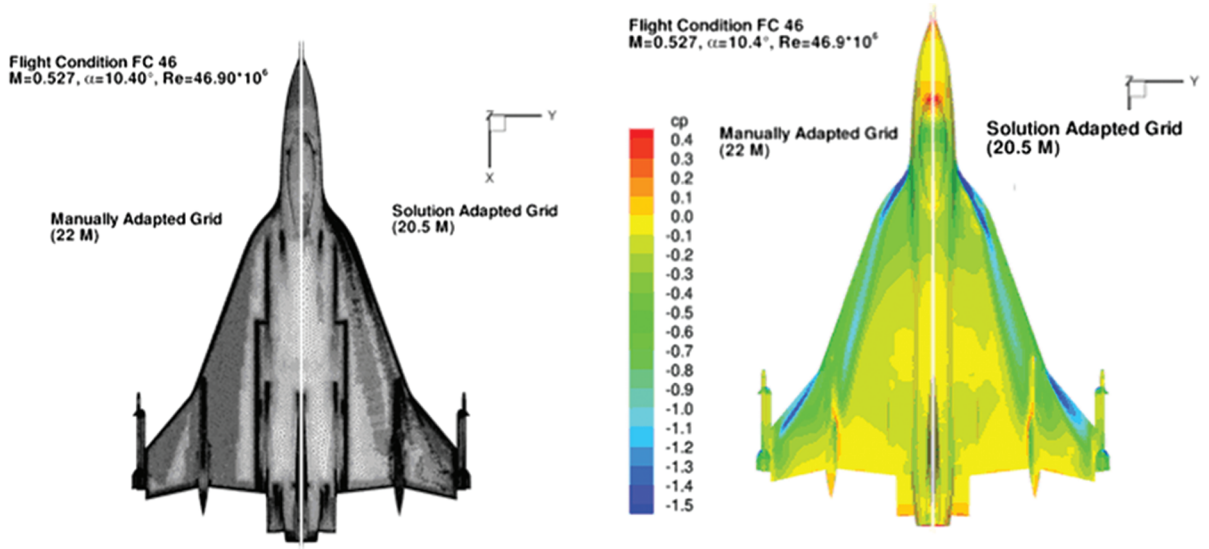

Fig. 21 Solution-adaptive grid effect for FC46 with TAU solver from Fritz [23].

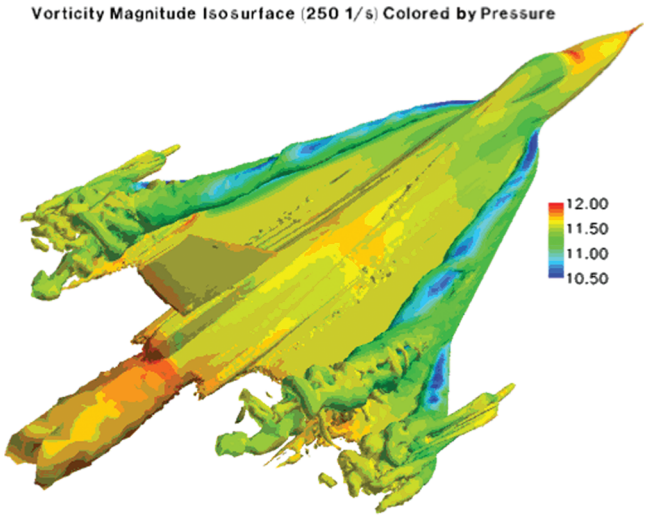

Fig. 22 Time-accurate solution for FC19 with Cobalt solver from Morton et al. [24].

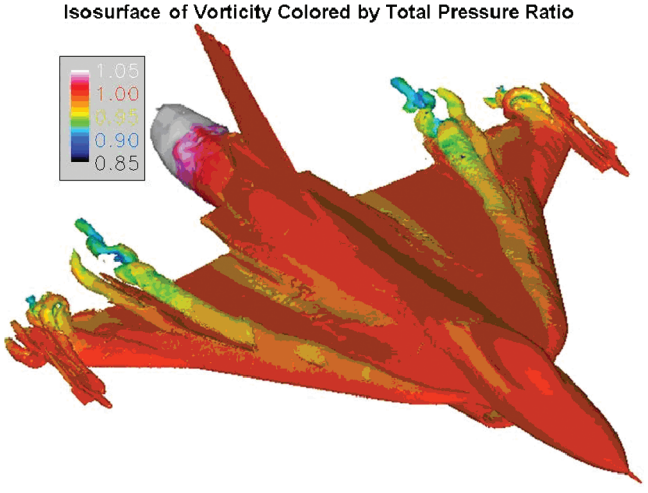

Fig. 23 Time-dependent solution for FC 7 with BCFD solver from Michal et al. [26].

three objectives to be performed under this task among the participants. They are detailed as follows:

1) Assess the various CFD codes against F-16XL-1 flight, and perhaps wind-tunnel, data sets to increase the Technology Readiness Level of the respective codes to a value of 5 (component and/or breadboard verification in a relevant environment).

2) Develop the best practices for each code based on the data sets.

3) Incorporate appropriate or upgraded turbulence models into the respective codes to provide for improved agreement.

These were to be accomplished by having each of the participating groups be responsible for certain aspects of the work. For example, each participating group would use their best efforts, consistent with program priorities and funding, to perform the agreed upon detailed tasks and to be responsible for providing its own resources for the completion of this task. In particular, NASA agreed to do the following:

1) Supply export-controlled geometry in various formats [Initial Graphics Exchange Specification (IGES), structured grid, and

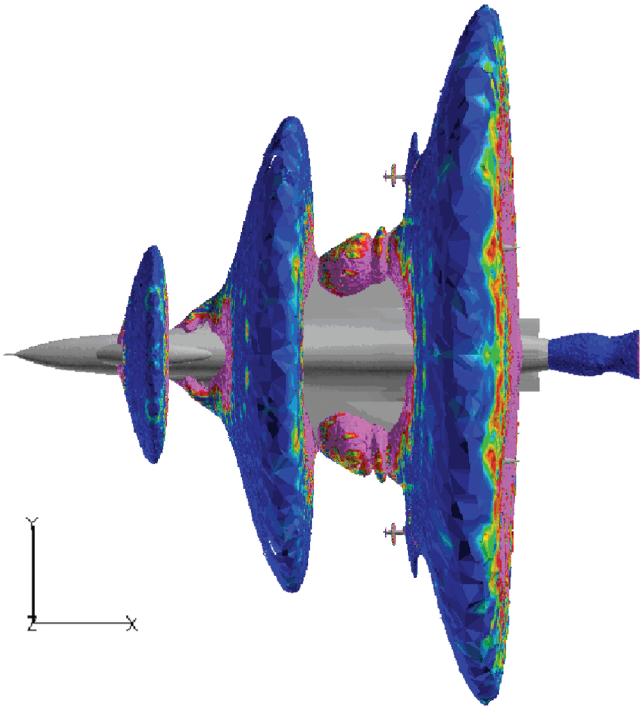

Fig. 24 Mach 1 isosurface colored by total pressure at FC 70 with Falcon v4 solver from Davis et al. [27].

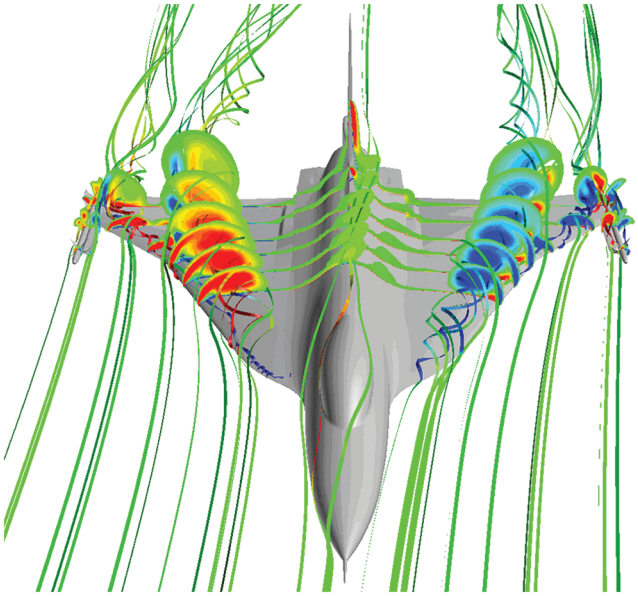

Fig. 25 Pressure-colored streamlines and *x*-vorticity component for FC50 with TENASI solver from Karman et al. [28].

unstructured grid] of the F-16XL-1 aircraft to participating partners once a formal memorandum of agreements is in place.

2) Make available flight pressures, images, and skin-friction and boundary-layer measurements to the team.

3) Supply data format to, and coordinate database services needed by, the group.

4) Coordinate the various efforts and arrange for meetings each 6 months in conjunction with the RTO symposium.

5) The completion date of this task should be a maximum of 3 years after all approvals are granted. The initial ending date was set for December 2005, but this was later extended to December 2007, due to a variety of factors.

The fact that the aircraft geometry was restricted by International Traffic in Arms Regulations complicated the process of NASA fulfilling its obligations until it was realized that a virtual laboratory, housed in an electronically secure demilitarized zone, was a solution for geometry and grid transfers among participants. Details about this have been documented [17,18]. Accessibility to both old and new data was provided through the VL to the participants. After the conclusion of the task group, it was anticipated that portions of the database would be made widely available via the VL, but that is highly unlikely given the current environment.

The CAWAPI facet work was facilitated by having well-known and highly respected organizations/researchers as members of this international effort working under the RTO umbrella. These organizations appear in the following list, grouped according to their basic function. They include four airframe companies: Boeing—St. Louis Phantom Works (United States), EADS—Munich (Germany), Lockheed Martin Aeronautics Company—Fort Worth (United States), and Turkish Aircraft Industries (Turkey); two government research laboratories: LaRC (United States) and National Aerospace Laboratory/NLR (The Netherlands); and six university-led efforts: Royal Institute of Technology /Swedish Defence Research Agency (Sweden), U.S. Air Force Academy (United States), University of Glasgow/Liverpool University (United Kingdom), University of Tennessee—Chattanooga/SimCenter (United States), University of Wyoming (United States), and Vrije Universiteit Brussel/Numeca (Belgium). Unfortunately, not all of these were able to continue to the end of this facet, and some optioned to continue in the VFE-2 facet instead.

Sample Results

The original CAWAP solutions were obtained using a structured grid solver, based on a documented IGES file with refinements, compared with measured flight data, and reported in [2] for the F-16XL-1 aircraft. It was anticipated that the new solutions would employ both structured and unstructured grids. Rather than just use the same IGES file as before, it was decided to reinvestigate the geometry, find the best IGES file available, and make certain that it was equally suitable for both solver types. The new IGES file is only slightly different from the previous one, but it satisfied both grid communities. The process of obtaining grids for both structured and unstructured solvers from this IGES file is detailed in [19], and Fig. 15 is a sample from that paper.

When the CAWAPI computational effort commenced, the majority of those performing computations planned to do so using structured grid solvers; however, in the ensuing years, that trend has reversed and now the majority are using unstructured grid solvers. A partial reason for this movement has been the improvements made in

Table 4 Seven flight conditions to be examined

Flight condition	Actual Mach number	Actual α, deg	Actual β, deg	Actual Reynolds number
FC7	0.304	11.89	−0.133	44.4×10^6
FC19	0.36	11.85	0.612	46.8×10^6
FC46	0.527	10.4	0.684	46.9×10^6
FC70	0.97	4.37	0.310	88.77×10^6
FC25	0.242	19.84	0.725	32.22×10^6
FC50	0.434	13.56	5.31	39.41×10^6
FC51	0.441	12.89	−4.58	38.95×10^6

Table 5 Associated engine parameters[a] for flight conditions

Flight condition	Freestream altitude, ft	Freestream Mach number	Inlet-duct-exit static temperature, °R	Inlet-duct-exit static pressure, psia	Inlet-duct-exit velocity, ft/s	Inlet-duct-exit Mach number	Mixing-plane total temperature, °R	Mixing-plane total pressure, psia
FC7	5000	0.304	498	11	379.6	0.347	1050	23
FC19	10,000	0.36	485.8	10.2	345.8	0.32	1050	21.5
FC46	24,000	0.527	443.6	5.85	404.3	0.39	1045	14.8
FC70	22,300	0.97	519	10.65	464.7	0.416	1200	30
FC25	10,000	0.242	470.1	8.72	474.8	0.447	1209	26.3
FC50	24,000	0.434	440	5.16	483.3	0.47	1154	16.95
FC51	24,000	0.441	431.8	5.19	468.6	0.46	1146	16.74

[a]The numbers in this table do not represent any particular engine.

these solvers that include the potential and actualization of breaking a solution down into components for parallel processing and the potential for automatic grid generation. Both of these can lead to significant time reductions from geometry specification to solver results. In the listing of papers that follows, authors have used their solvers (structured [20–22] or unstructured [23–29]) to determine the best practices for each code and type of flow combination and then made comparisons with each other's predictions or flight data as they deemed appropriate. Each of these papers has its own focus, but also contains common comparisons. For example, [20] emphasizes surface streamlines and understanding the relation with the off-surface flow, as shown by the sample Fig. 16. A variety of aircraft modeling studies were performed in [21], with the results for the complete aircraft shown in Fig. 17. References [22,25,29] emphasize the effects of various turbulence models and are shown by sample Figs. 18–20, respectively. Figure 20 [29] also shows, for comparison, the flight data represented by small circles surrounding the pressure-port locations, shown as black dots, and colored by the CFD C_p scale. Reference [23] emphasizes solution-adaptive grids, as shown by the sample Fig. 21. References [24,26] highlight time-accurate, time-dependent, and time-averaged solutions and are illustrated in Figs. 22 and 23, respectively. Figure 24 [27] shows the Mach 1 isosurface colored by total pressure at FC 70. Figure 25 [28] shows streamlines and the x-vorticity component for FC50, where $\beta = +5.31$ deg. Finally, [30] provides a summary of the lessons learned as a result of this computational effort, including its impact on the Technology Readiness Level of the examined current solvers.

Please note that all of the referenced papers have been summarized into the following five articles in this "Prediction of F-16XL Flight Flow Physics" special section. These articles follow the same general arrangement as the conference papers in that the next paper in this sequence is the geometry/grid discussion [31], followed by solutions for the structured grid [32], unstructured standard grid [33], unstructured tailored grid [34], and a concluding article on the lessons learned [35]. Each of these articles has a lead author who planned the scope and coordinated the efforts of the coauthors.

An initial group of four flight conditions with either vortex-dominated or transonic flows were adopted by this facet for prediction and comparison. These were later expanded to seven and included two sideslip conditions (see Table 4). Associated with each was a set of pressure/temperature/Mach number values for a generic engine (see Table 5).

Conclusions

1) Aircraft companies, government laboratories, and universities have access to database sets that may include flight data, but many of these sets are considered proprietary and are only used by them to assess and improve their codes. They hold this information in a closed environment to maintain a competitive advantage. The CAWAP data set, being open, allowed researchers in these organizations to predict flight data in a cooperative manner under the RTO umbrella and facilitate doctoral studies.

2) There is interest in the international aeronautical community (airframe companies, government laboratories, and universities) in being able to predict the flow physics measured on a fighter aircraft.

3) An international team of experts can be assembled with enough patience and institutional support when there is a focused common problem of mutual interest that can provide positive payoff for each organization.

4) The efforts expended by the participating organizations/researchers described here have led to the development of improved use or best practices for their flow solvers for the F-16XL aircraft. Moreover, an improvement in the ability (Technology Readiness Level) of organizations/researchers to predict complete fighter aircraft flow physics at real flight conditions has occurred, in part, due to their participating in this shared and open environment.

5) The preceding leads to the observation that focused data sets should be collected on aircraft configuration(s) of international aeronautical community interest without geometrical restriction under the RTO umbrella for similar CFD solver improvement.

This paper has traced the F-16XL-1 aircraft and the flight flow-physics data from a NASA-only activity to encompass others in the NATO community who are interested in predicting these data. The Cranked-Arrow Wing Aerodynamics Project (CAWAP) has been internationalized under the auspices of the RTO, the scientific arm of NATO, and the Technology Readiness Level of computational tools has been increased. Sample results obtained by CAWAPI facet members have been highlighted to show the breadth of work presented by them in their own AIAA papers or in the following summary articles.

Acknowledgments

The Cranked-Arrow Wing Aerodynamics Project International facet gratefully acknowledges the support provided by Lockheed Martin Aeronautics Company—Fort Worth in providing a refined Initial Graphics Exchange Specification (IGES) geometry file and the parameter values of a generic engine that were subsequently used by facet members in their computational fluid dynamics studies, and the geometrical work performed by Edward B. Parlette of Vigyan, Inc., in generating a series of unstructured tetrahedral grids from the IGES file, with the last one known as the base grid.

References

[1] Bertin, J. J., and Smith, M. L., *Aerodynamics for Engineers*, 2nd ed., Prentice–Hall, Upper Saddle River, NJ, 1989, p. 146.

[2] Lamar, J. E., Obara, C. J., Fisher, B. D., and Fisher, D. F., "Flight, Wind-Tunnel, and Computational Fluid Dynamics Comparison for Cranked Arrow Wing (F-16XL-1) at Subsonic and Transonic Speeds," NASA TP-2001-210629, Feb. 2001.

[3] Hillaker, H. J., "F-16XL Flight Test Program Overview," AIAA Paper 83-2730, Nov. 1983.

[4] Bower, J. N., and Scott, S. R., "The F-16XL Flight Test Program," *15th Annual Symposium Proceedings*, Society of Flight Test Engineers, Lancaster, CA, Aug. 1984, pp. 9-1–9-5.

[5] Talty, P. K., and Caughlin, D. J., "F-16XL Demonstrates New Capabilities in Flight Test at Edwards Air Force Base," *Journal of Aircraft*, Vol. 25, No. 3, Mar. 1988, pp. 206–215. doi:10.2514/3.45579

[6] Bertelrud, A., "Total Head/Static Measurements of Skin Friction and Surface Pressure," *AIAA Journal*, Vol. 15, No. 3, Mar. 1977, pp. 436–438. doi:10.2514/3.7337

[7] Lamar, J. E., Obara, C. J., Fisher, B. D., and Fisher, D. F., "Flight, Wind-Tunnel, and Computational Fluid Dynamics Comparison for Cranked Arrow Wing (F-16XL-1) at Subsonic and Transonic Speeds," NASA TP-2001-210629/Supplement, June 2008.

[8] Thomas, J. L., Anderson, W. K., and Krist, S. T., "Navier–Stokes Computations of Vortical Flows over Low-Aspect-Ratio Wings," *AIAA Journal*, Vol. 28, No. 2, Feb. 1990, pp. 205–212. doi:10.2514/3.10376

[9] Thomas, J. L., Weston, R. P., Luckring, J. M., Walters, R. W., Reu, T., and Ghaffari, F., "A Patch-Grid Algorithm for Complex Configurations Directed Towards the F-18 Aircraft," AIAA Paper 89-121, 1989.

[10] Spellman, M. W., "Model and Test Information Report 1/9-Scale F-16E Force and Loads Model," General Dynamics Corp., Rept. 400PR026, Ft. Worth, TX, Aug. 1981.

[11] Elbers, W. K., "Wind Tunnel Data Report 1/9-Scale F-16E Pressure Model NASA Ames Research Center Tests 517-1-11 and 517-1-97," General Dynamics Corp. Rept. 400PR037, Vol. 2, Ft. Worth, TX, Dec. 1981.

[12] Hahne, D. E., "Low-Speed Aerodynamic Data for an 0.18-Scale Model of an F-16XL with Various Leading-Edge Modifications," NASA TM-1999-209703, 1999.

[13] Lessard, W. B., "Subsonic Analysis of 0.04-Scaled F-16XL Models Using an Unstructured Euler Code," NASA TP-3597, 1996.

[14] White, F. M., *Viscous Fluid Flow*, McGraw–Hill, New York, 1974, pp. 474–476.

[15] Lamar, John, E., "Cranked Arrow Wing (F-16XL-1) Flight Flow Physics with CFD Predictions at Subsonic and Transonic Speeds," *RTO AVT Symposium on Advanced Flow Management: Part A—Vortex Flow and High Angle of Attack*, Research and Technology Organization Paper 44, May 2001.

[16] Hummel, D., and Redeker, G., "A New Vortex Flow Experiment for Computer Code Validation," *RTO AVT Symposium on Advanced Flow*

Management: Part A—Vortex Flow and High Angle of Attack, Research and Technology Organization Paper 8, May 2001.

[17] Lamar, J. E., Conin, C. K., and Scott, Laura, E., "A Review of Steps Taken to Create an International Virtual Laboratory at NASA Langley for Aerodynamic Prediction and Comparison," *Progress in Aerospace Sciences*, Vol. 40, p. 163–172. doi:10.1016/j.paerosci.2004.03.002, 2004.

[18] Lamar, John, E., Cronin, C. K., and Scott, L. E., "Virtual Laboratory Enabling Collaborative Research in Applied Vehicle Technologies," *AVT-123 Symposium on Flow Induced Unsteady Loads and the Impact on Military Applications*, Research and Technology Organization, Keynote 2, Apr. 2005.

[19] Boelens, O. J., Goertz, S., Morton, S. A., Fritz, W., and Lamar, J. E., "Description of the F-16XL Geometry and Computational Grids Used in CAWAPI," AIAA Paper 2007-488, Jan. 2007.

[20] Boelens, O. J., Spekreijse, S. P., Sytsma, H. A., and de Cock K. M. J., "Comparison of Measured and Simulated Flow Features for the Full-Scale F-16XL Aircraft," AIAA Paper 2007-489, Jan. 2007.

[21] Badcock K. J., "Evaluation of Results from a Reynolds Averaged Multiblock Code Against F-16XL Flight Data," AIAA Paper 2007-490, Jan. 2007.

[22] Elmiligui, A. A., Abdol-Hamid, K. S., and Massey, S. J., "PAB3D Simulations for the CAWAPI F-16XL," AIAA Paper 2007-491, Jan. 2007.

[23] Fritz, W., "Hybrid Grid RANS Solutions for the CAWAPI F-16XL," AIAA Paper 2007-492, Jan. 2007.

[24] Morton. S. A., McDaniels, D. R., and Cummings, R. M., "F-16XL Unsteady Simulations for the CAWAPI Facet of RTO Task Group AVT-113," AIAA Paper 2007-493, Jan. 2007.

[25] Goertz, S., and Jirásek, A., "Unstructured Steady/Unsteady Solutions with Edge for CAWAPI F-16XL at KTH/FOI," AIAA Paper 2007-678, Jan. 2007.

[26] Michal, T., Oser, M., Mani, M., and Roos, F., "BCFD Unstructured-Grid Predictions on the F-16XL (CAWAPI) Aircraft," AIAA Paper 2007-679, Jan. 2007.

[27] Davis, M. B., Reed, C., and Yagle, P., "Hybrid Grid Solutions on the (CAWAPI) F-16XL Using Falcon v4," AIAA Paper 2007-680, Jan. 2007.

[28] Karman, S. L., Jr., Mitchell, B., and Sawyer, S., "Unstructured Grid Solutions of CAWAPI F-16XL by UT SimCenter," AIAA Paper 2007-681, Jan. 2007.

[29] Lamar, J. E., and Abdol-Hamid, K. S., "USM3D Unstructured Grid Solutions for CAWAPI at NASA LaRC," AIAA Paper 2007-682, Jan. 2007.

[30] Rizzi, A., Badcock K., Jirásek, A., and Boelens, O., "What Was Learned from Numerical Simulations of F-16XL (CAWAPI) at Flight Conditions," AIAA Paper 2007-683, Jan. 2007.

[31] Boelens, O. J., Goertz, S., Morton, S. A., Fritz, W., and Lamar, J. E., "Description of the F-16XL Geometry and Computational Grids Used in CAWAPI," *Journal of Aircraft*, Vol. 46, No. 2, 2009, pp. 369–376. doi:10.2514/1.34852

[32] Boelens, O. J., Badcock K. J., Elmilgui, A., Abdol-Hamid, K. S., and Massey, S. J., "Comparison of Measured and Block Structured Simulations for the F-16XL Aircraft," *Journal of Aircraft*, Vol. 46, No. 2, 2009, pp. 377–384. doi:10.2514/1.35064

[33] Goertz, S., Jirásek, A., Morton, S. A., McDaniels, D. R., Cummings, R. M., Lamar, J. E., and Abdol-Hamid, K. S., "Standard Unstructured Grid Solutions for CAWAPI F-16XL," *Journal of Aircraft*, Vol. 46, No. 2, 2009, pp. 385–408. doi:10.2514/1.35163

[34] Fritz, W., Davis, M. B., Karman, S. L., Jr., and Michal, T., "RANS Solutions for the CAWAPI F-16XL Using Different Hybrid Grids," *Journal of Aircraft*, Vol. 46, No. 2, 2009, pp. 409–422. doi:10.2514/1.35106

[35] Rizzi, A., Jirásek, A., Lamar, J. E., Crippa, S., Badcock K. J., and Boelens, O. J., "Lessons Learned from Numerical Simulations of the F-16XL Aircraft at Flight Conditions," *Journal of Aircraft*, Vol. 46, No. 2, 2009, pp. 423–441. doi:10.2514/1.35698